American Mineralogist, Volume 101, pages 461–468, 2016

Ferri-kaersutite, $NaCa_2(Mg_3TiFe^{3+})(Si_6Al_2)O_{22}O_2$, a new oxo-amphibole from Harrow Peaks, Northern Victoria Land, Antarctica

Silvia Gentili[1,*], Cristian Biagioni[2], Paola Comodi[1], Marco Pasero[2], Catherine McCammon[3], and Costanza Bonadiman[4]

[1]Dipartimento di Fisica e Geologia, Università di Perugia, Piazza dell'Università 1, 06123 Perugia, Italy
[2]Dipartimento di Scienze della Terra, Università di Pisa, Via Santa Maria 53, 56126 Pisa, Italy
[3]Bayerisches Geoinstitut, Universität Bayreuth, 95440 Bayreuth, Germany
[4]Dipartimento di Fisica e Scienze della Terra, Via Saragat 1, 44122 Ferrara, Italy

Abstract

Ferri-kaersutite, ideally $NaCa_2(Mg_3TiFe^{3+})(Si_6Al_2)O_{22}O_2$, is a new oxo-amphibole from Harrow Peaks, Northern Victoria Land, Antarctica. It occurs as brown prismatic crystals, up to 200 μm in length, with a vitreous luster, and a perfect {110} cleavage. Ferri-kaersutite is associated with forsterite, diopside, and Cr-bearing spinel. Chemical analyses, by a combination of electron microprobe, SIMS, and ^{57}Fe Mössbauer spectroscopy, gave the following results (in wt%): SiO_2 41.69, TiO_2 5.30, Al_2O_3 13.65, Cr_2O_3 0.09, Fe_2O_3 4.52, MgO 15.54, CaO 11.03, MnO 0.11, FeO 2.83, Na_2O 2.88, K_2O 0.96, H_2O 0.70, F 0.24, Cl 0.08, O=(F,Cl) –0.12, sum 99.50. On the basis of 24 anions per formula unit, the formula is $(Na_{0.816}K_{0.179})_{\Sigma 0.995}(Ca_{1.726}Fe^{2+}_{0.258}Mn_{0.014})_{\Sigma 1.998}(Mg_{3.383}Fe^{2+}_{0.088}Ti_{0.582}Fe^{3+}_{0.497}Al_{0.439}Cr_{0.011})_{\Sigma 5.00}(Si_{6.089}Al_{1.911})_{\Sigma 8.00}O_{22}[O_{1.187}(OH)_{0.682}F_{0.111}Cl_{0.020}]_{\Sigma 2.00}$. Ferri-kaersutite is monoclinic with space group *C*2/*m*. Its unit-cell parameters are a = 9.8378(8), b = 18.0562(9), c = 5.3027(4) Å, β = 105.199(9)°, V = 908.99(13) Å^3, Z = 2. The five strongest reflections in its X-ray powder diffraction pattern [d in Å (relative visual intensity, *hkl*)] are: 8.4 (s, 110), 3.379 (ms, 131), 3.115 (ms, 310), 2.707 (s, 151), 2.598 (ms, 061). The crystal structure of ferri-kaersutite has been refined on the basis of 1783 observed reflections [$F_o > 4\sigma(F_o)$] with a final R_1 = 0.038.

The relatively large equivalent isotropic displacement parameter at *M*(1), with respect to those at *M*(2) and *M*(3) sites, together with the short *M*(1)–O(3) distance, suggest the occurrence of Ti^{4+} at the *M*(1) site, whereas the small octahedral distortion at this site suggests a low Fe^{3+} occupancy. This element is mainly hosted at the *M*(2) and *M*(3) sites.

The occurrence of amphiboles in the magma source region is notably relevant. The melting of Ti-rich amphibole in the lithosphere and subsequent degrees of melt/host peridotite reactions are able to produce melts that account for the compositional spectrum ranging from extreme alkaline lavas to the most common alkaline basalts. In particular, when this amphibole is formed by reaction between a peridotite matrix and metasomatic melts/fluids with high Fe^{3+}/Fe_{tot} ratio, its subsequent melting can influence primary volatile contents and ultimately magma rheology.

Keywords: Ferri-kaersutite, new mineral, crystal chemistry, oxo-amphibole, Victoria Land, Antarctica

Introduction

Among the 93 currently valid mineral species within the amphibole supergroup (http://ima-cnmnc.nrm.se/imalist.htm; IMA list of minerals), only seven belong to the oxo-amphibole group (Table 1), i.e., amphiboles having $^{W}O^{2-} > {}^{W}(OH+F+Cl)^-$.

A mineralogical and petrological study of amphiboles occurring in mantle xenoliths from Harrow Peaks, Victoria Land, Antarctica, revealed the presence of an amphibole approaching the end-member formula $NaCa_2(Mg_3TiFe^{3+})(Si_6Al_2)O_{22}O_2$, i.e., ferri-kaersutite according to the new amphibole nomenclature (Hawthorne et al. 2012).

Previously a mineral belonging to the oxo-amphibole group was submitted to the IMA CNMNC and approved with the name ferrikaersutite (IMA 2011-035; Zaitsev et al. 2011). Shortly thereafter, following the new IMA report on the nomenclature of the amphibole supergroup (Hawthorne et al. 2012), both the assigned name and the end-member formula were found to be wrong. Therefore, IMA 2011-035 was renamed oxo-magnesio-hastingsite, with ideal formula $NaCa_2(Mg_2Fe^{3+}_3)(Si_6Al_2)O_{22}O_2$ (Zaitsev et al. 2013).

The aim of this paper is the description of the new mineral ferri-kaersutite from Harrow Peaks, Victoria Land, Antarctica. The mineral and its name have been approved by the IMA-CNMNC, under the number IMA 2014-051. The holotype material is deposited in the mineralogical collections of the Museo di Storia Naturale, University of Pisa, via Roma 79, Calci, Pisa, Italy, under catalog number 19689.

* E-mail: silvia.gentili@studenti.unipg.it

0003-004X/16/0002–461$05.00/DOI: http://dx.doi.org/10.2138/am-2016-5204

Table 1. Valid species belonging to the oxo-amphibole group

Mineral species	Chemical formula	Ref.
Ferro-ferri-obertiite	$NaNa_2(Fe^{2+}_3TiFe^{3+})Si_8O_{22}O_2$	(1)
Kaersutite	$NaCa_2(Mg_3TiAl)(Si_6Al_2)O_{22}O_2$	(2)
Mangani-dellaventuraite	$NaNa_2(MgMn^{3+}_2TiLi)Si_8O_{22}O_2$	(3)
Mangani-obertiite	$NaNa_2(Mg_3TiMn^{3+})Si_8O_{22}O_2$	(4)
Mangano-mangani-ungarettiite	$NaNa_2(Mn^{2+}_2Mn^{3+}_3)Si_8O_{22}O_2$	(5)
Oxo-magnesio-hastingsite	$NaCa_2(Mg_2Fe^{3+}_3)(Si_6Al_2)O_{22}O_2$	(6)
Oxo-mangani-leakeite	$NaNa_2(Mn^{3+}_4Li)Si_8O_{22}O_2$	(7)

Note: (1) Hawthorne et al. 2010; (2) Comodi et al. 2010; (3) Tait et al. 2005; (4) Hawthorne et al. 2000; (5) Hawthorne et al. 1995a; (6) Zaitsev et al. 2013; (7) Oberti et al. 2015.

Occurrence

Ferri-kaersutite was identified in an ultramafic xenolith occurring in Cenozoic alkaline mafic lava from Harrow Peaks, Northern Victoria Land (NVL), Antarctica (latitude 74.02785°S, longitude 164.47466°E, 335 m above sea level; Fig. 1). The Cenozoic igneous activity in NVL was related to the West Antarctic Rift System and it was characterized by intrusions, dike swarms, and volcanoes (Fitzgerald et al. 1987; Wörner 1999; Rocchi et al. 2002). Mantle xenoliths, brought to the surface by alkaline magmas, revealed upper mantle heterogeneities in this area, which result from combined effects of partial melting episodes and diffuse metasomatic enrichment (Zipfel and Wörner 1992; Coltorti et al. 2004; Perinelli et al. 2006, 2012; Melchiorre et al. 2011; Bonadiman et al. 2014; Gentili et al. 2015). The occurrence of amphiboles in mantle parageneses is particularly intriguing because their crystal chemistry is closely related to the chemical-physical conditions of the percolating fluids at upper mantle level.

Ferri-kaersutite was found in a spinel-bearing lherzolite having a 5 cm diameter. The sample shows a protogranular texture (Mercier and Nicolas 1975) and, accordingly, it does not show any pronounced fabric orientation. The mineral assemblage

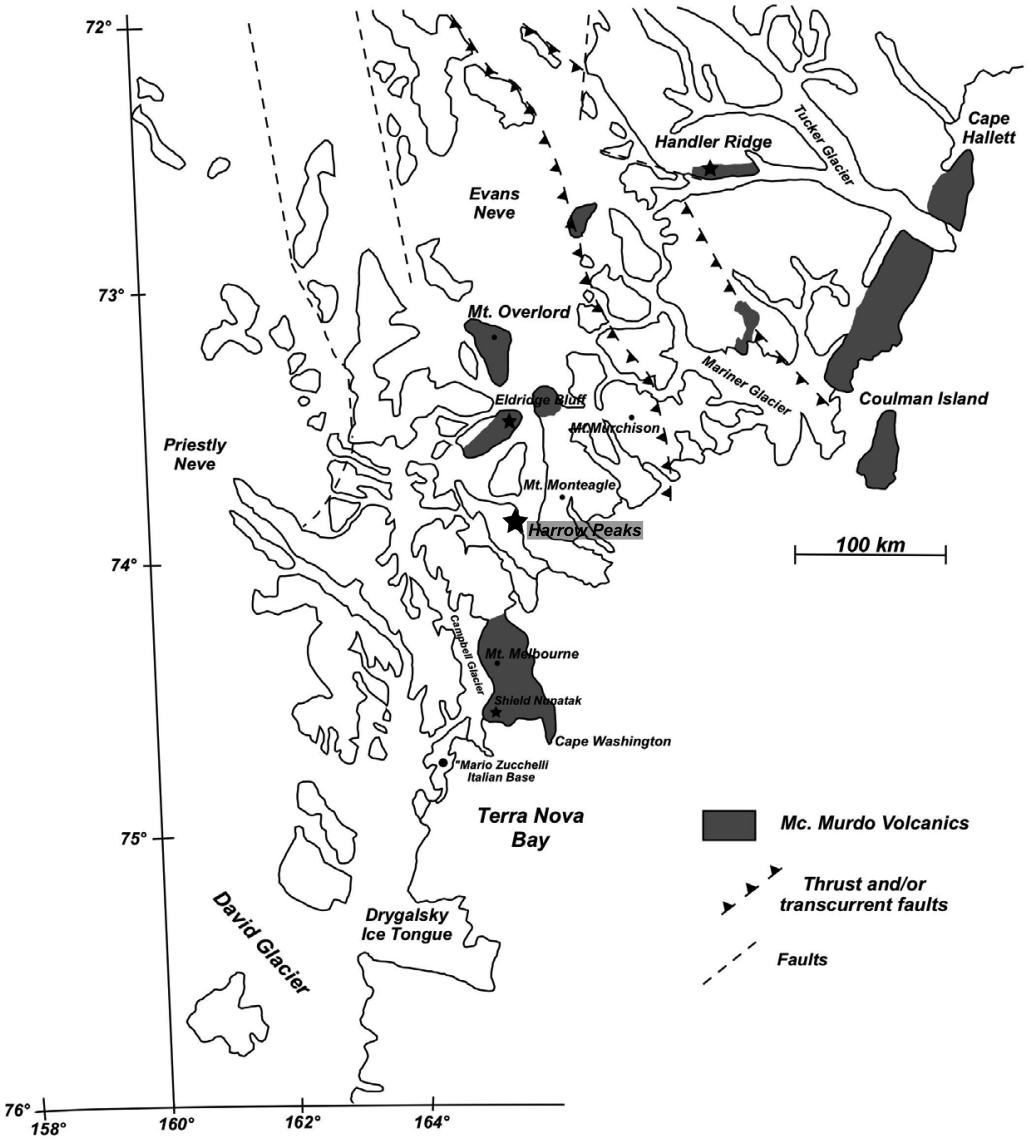

Figure 1. Location map of Northern Victoria Land (after Giacomoni et al. 2013).

does not provide any evidence of infiltration of the host basalt or superficial alteration. Amphibole occurs as disseminated grains texturally related to diopside and Cr-bearing spinel, as observed in the nearby xenoliths population from Baker Rocks and Greene Point (Coltorti et al. 2004; Perinelli et al. 2012; Bonadiman et al. 2014).

Mineral description

Ferri-kaersutite occurs as brown euhedral prismatic crystals, up to 200 μm in length. It has a vitreous luster. It is brittle, with a perfect {110} cleavage. Owing to the very low amount of available material (only two grains), some physical properties could not be measured, such as streak, micro-hardness, density, and optical properties. Calculated density, based on the empirical formula (see below) is 3.190 g/cm^3, whereas the density corresponding to the end-member formula is 3.237 g/cm^3.

Chemical composition

Quantitative chemical analyses of ferri-kaersutite were carried out using a CAMECA SX-50 electron microprobe operating in wavelength-dispersive mode, with accelerating voltage 15 kV, beam current 15 nA, and beam size 1 μm. The standards (element, emission line, counting times for peak positions) are: diopside (Si*K*α 10 s, Ca*K*α 10 s), synthetic $MnTiO_3$ (Ti*K*α 10 s, Mn*K*α 10 s), plagioclase (Na*K*α 10 s), orthoclase (K*K*α 7 s), periclase (Mg*K*α 10 s), corundum (Al*K*α 10 s), hematite (Fe*K*α 10 s), and synthetic Cr_2O_3 (Cr*K*α 10 s). Raw counts were processed using the PAP data reduction method (Pouchou and Pichoir 1985). The average of 10 spot analyses is given in Table 2. No chemical zoning was observed in the studied crystal.

Secondary ion mass spectroscopy (SIMS) measurements were performed with a CAMECA IMS 4f ion microprobe. A 12.5 kV accelerated ^{16}O-primary ion beam was used with a current intensity of 7–10 nA and ~10–15 μm beam diameter. The mounts of both the sample and the standards were left to degas overnight in the ion-microprobe sample chamber. Secondary ion signals of the following isotopes were monitored at the electron multiplier: $^1H^+$, $^{19}F^+$, $^{37}Cl^+$, and $^{30}Si^+$ (the latter was used as the internal reference for the matrix). Acquisition times were 20 s (H), 50 s (Cl), 50 s (F), and 15 s (Si) over five analytical cycles. Detection of positive secondary ions in the range of 75–125 eV emission kinetic energies was obtained under steady-state sputtering conditions after pre-sputtering. Mass calibration was checked before each analysis. Empirical corrections were adopted for the ''Ion Yields'' IY(H/Si) to account for the variation of the ion signals with increasing (Fe + Mn) content in the sample, as fully described by Ottolini et al. (2001, 2002). The precision of the H determination was estimated on the basis of the reproducibility of the standard analyses and was better than 8% (Ottolini et al. 1993, 1995). The overall accuracy of the volatile and light element determination at the concentration level exhibited by the samples of this work is better than 15%.

Finally, micro-Mössbauer spectroscopy was used for the determination of the Fe^{2+}-Fe^{3+} ratio. A Mössbauer spectrum (Fig. 2) was collected in transmission mode at room temperature on a constant acceleration Mössbauer spectrometer with a nominal 370 MBq ^{57}Co high specific activity source in a 12 μm thick Rh matrix. The velocity scale was calibrated relative to 25 μm thick α-Fe foil using the positions certified for (former) National Bureau of Standards standard reference material no. 1541. Mössbauer spectra were fitted to three Lorentzian doublets and the usual constraints were applied to all doublets (equal component areas and widths) using the program MossA (Prescher et al. 2012). Area asymmetry due to preferred orientation was explored and the value of Fe^{3+}/Fe_{tot} was calculated based on relative area ratios, where uncertainties were estimated based on fitting statistics. The preliminary Fe^{3+}/Fe_{tot} estimate of 59(7)% was used for structure and composition calculations, but this value was subsequently refined to 57(7)% from a spectrum with a longer collection time (Fig. 2). We note that the two values of Fe^{3+}/Fe_{tot} are indistinguishable within experimental uncertainty and there is no observable influence of the difference in values on any of the conclusions.

Table 2. Chemical composition of ferri-kaersutite (as wt%; average of 10 spot analyses) and number of atoms per formula unit (apfu) based on 24 anions per formula unit

Oxide	wt%	range	e.s.d.	Element	apfu	range	e.s.d.
SiO_2	41.69	41.29–41.90	0.29	Si^{4+}	6.089	6.053–6.125	0.024
TiO_2	5.30	5.23–5.44	0.09	Ti^{4+}	0.582	0.570–0.600	0.012
Al_2O_3	13.65	13.23–14.01	0.32	Al^{3+}	2.350	2.276–2.416	0.057
Cr_2O_3	0.09	0.08–0.12	0.02	Cr^{3+}	0.011	0.009–0.014	0.002
Fe_2O_3	4.52			Fe^{3+}	0.497	0.464–0.524	0.023
FeO	2.83			Fe^{2+}	0.346	0.322–0.364	0.016
FeO_{tot}	6.90	6.47–7.25	0.33				
MnO	0.11	0.08–0.13	0.02	Mn^{2+}	0.014	0.010–0.017	0.003
MgO	15.54	15.29–15.70	0.18	Mg^{2+}	3.383	3.331–3.445	0.042
CaO	11.03	10.94–11.20	0.12	Ca^{2+}	1.726	1.712–1.746	0.014
Na_2O	2.88	2.80–2.99	0.08	Na^+	0.816	0.788–0.847	0.022
K_2O	0.96	0.94–0.98	0.02	K^+	0.179	0.175–0.184	0.003
H_2O	0.70	0.65–0.72	0.03	OH^-	0.682	0.678–0.687	0.003
F	0.24	0.23–0.27	0.02	F^-	0.111	0.110–0.112	0.000
Cl	0.08	0.07–0.08	0.01	Cl^-	0.020	0.020–0.020	0.000
Total	99.62	99.00–100.22	0.35	O^{2-}	23.187	23.181 – 23.192	0.004
O=F,Cl	–0.12						
Sum	99.50	98.88–100.10	0.35				

Note: FeO_{tot} (wt%) from microprobe analysis; Fe_2O_3 and FeO (wt%) from Mössbauer spectroscopy; F (wt%), Cl (wt%), and H_2O (wt%) from SIMS.

The chemical formula based on 24 anions (O, OH, F, Cl) was

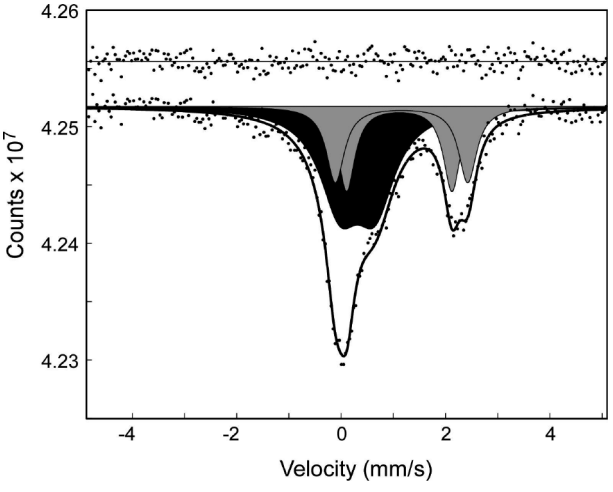

Figure 2. Room-temperature Mössbauer spectrum of ferri-kaersutite. The doublets assigned to Fe^{2+} and Fe^{3+} are shaded gray and black, respectively.

calculated using the value of Fe^{3+}/Fe_{tot} of 59(7)% measured by micro-Mössbauer and OH, F, and Cl measured by SIMS (Table 2). All manganese was assumed as Mn^{2+}, even if in other oxo-amphiboles (e.g., mangano-mangani-ungarettiite) manganese is known to partially occur as Mn^{3+}. However, owing to its very low content (0.01 atoms per formula unit, apfu), the oxidation state of manganese is not a crucial factor for classification purposes.

The empirical formula of ferri-kaersutite is: $(Na_{0.816}K_{0.179})_{\Sigma 0.995}(Ca_{1.726}Fe^{2+}_{0.258}Mn_{0.014})_{\Sigma 1.998}(Mg_{3.383}Fe^{2+}_{0.088}Fe^{3+}_{0.497}Al_{0.439}Cr_{0.011}Ti_{0.582})_{\Sigma 5.00}(Si_{6.089}Al_{1.911})_{\Sigma 8.00}O_{22}[O_{1.187}(OH)_{0.682}F_{0.111}Cl_{0.020}]_{\Sigma 2.00}$. The ideal formula is $NaCa_2(Mg_3Fe^{3+}Ti)(Si_6Al_2)O_{22}O_2$, which requires SiO_2 40.68, Fe_2O_3 9.01, MgO 13.64, TiO_2 9.01, CaO 12.65, Na_2O 3.50, total 100.00 wt%.

X-RAY CRYSTALLOGRAPHY AND STRUCTURE REFINEMENT

A quasi-powder X-ray diffraction pattern of ferri-kaersutite was obtained using a 114.6 mm diameter Gandolfi camera and Ni-filtered Cu*K*α radiation. The observed X-ray powder pattern is compared in Table 3 with that calculated using the software Powder Cell (Kraus and Nolze 1996). Unit-cell parameters, refined using UnitCell (Holland and Redfern 1997), are a = 9.845(11), b = 18.064(10), c = 5.312(6) Å, β = 105.26(10)°, V = 911.3(2) Å^3.

Single-crystal X-ray diffraction data were collected using an Xcalibur diffractometer equipped with a CCD area detector. Graphite-monochromatized Mo*K*α radiation was used. Data reduction was performed by using the package of software XcrysAlis (Agilent Technologies) and an empirical absorption correction was applied by the ABSPACK software as implement in XcrysAlis (Agilent Technologies). A statistical test ($|E^2 - 1|$ = 1.151) and systematic absences unequivocally confirmed the space group *C*2/*m*. Refined unit-cell parameters are a = 9.8378(8), b = 18.0562(9), c = 5.3027(4) Å, β = 105.199(9)°, V = 908.99(13) Å^3. The *a*:*b*:*c* ratio, calculated from single-crystal data, is 0.545:1:0.294.

The crystal structure of ferri-kaersutite was refined using SHELXL-97 (Sheldrick 2008) starting from the atomic coordinates of kaersutite (Comodi et al. 2010). Scattering curves for neutral atoms were taken from the *International Tables for Crystallography* (Wilson 1992). The occupancies of the cation sites were refined using the following scattering curves: *M*(1), *M*(2), *M*(3) sites: Mg vs. Fe; *M*(4) site: Ca vs. □; *M*(4′): Fe vs. □; *A* sites: Na vs. □; *T*(1), *T*(2) sites: Si vs. □. *T*(1) and *T*(2) were found fully occupied by Si and their site occupancies were then fixed on the basis of chemical data, calculating the $^{T(1)}$Al content on the basis of the relationship proposed by Oberti et al. (2007). The correct positions of the *M*(4′) and the split *A* sites, i.e., *A*(*m*) and *A*(2), were found by difference-Fourier maps. After several cycles of isotropic refinement, the R_1 value converged to 0.083. By introducing anisotropic displacement parameters for the cation sites, the refinement converged to R_1 = 0.047. Finally, anisotropic displacement parameters of anions were introduced. The refinement converged to the final R_1 value of 0.038. In the difference-Fourier maps, the highest maximum is at 0.67 Å from O(3), possibly related to the occurrence of a partially occupied H position at coordinates (0.18, 0, 0.73). These atom coordinates are similar to those expected for the H atom, even if the corresponding H–O distance is too short. Details of the crystal structure refinement are given in Table 4, whereas atomic coordinates and anisotropic displacement parameters are shown in Table 5. Table 6 gives selected bond distances for cation sites. (The CIF is available as Supplemental Material[1].)

TABLE 3. X-ray powder diffraction data for ferri-kaersutite

I_{obs}	d_{obs}	I_{calc}	d_{calc}	*h k l*	
–	–	18	9.03	0 2 0	
s	**8.4**	**70**	**8.40**	**1 1 0**	[a]
vw	4.85	16	4.91	$\bar{1}$ 1 1	
vw	4.52	18	4.51	0 4 0	[a]
vw	4.229				
–	–	14	3.890	$\bar{1}$ 3 1	
vw	3.703				
ms	**3.379**	**67**	**3.377**	**1 3 1**	[a]
m	3.266	47	3.271	2 4 0	[a]
ms	**3.115**	**78**	**3.117**	**3 1 0**	[a]
vw	3.035	4	3.033	$\bar{3}$ 1 1	[a]
m	2.938	42	2.931	2 2 1	[a]
vw	2.867				
vw	2.806	13	2.801	$\bar{3}$ 3 0	[a]
w	2.739	33	2.739	$\bar{3}$ 3 1	[a]
s	**2.707**	**100**	**2.704**	**1 5 1**	[a]
ms	**2.598**	**61**	**2.594**	**0 6 1**	[a]
–	–	72	2.549	$\bar{2}$ 0 2	
mw	2.344	42	2.342	$\bar{3}$ 5 1	[a]
w	2.336	18	2.326	$\bar{4}$ 2 1	
w	2.305	15	2.302	$\bar{1}$ 7 1	[a]
		18	2.289	$\bar{3}$ 1 2	
vw	2.221	8	2.219	$\bar{2}$ 4 2	[a]
mw	2.158	38	2.159	2 6 1	[a]
mw	2.041	21	2.040	$\bar{2}$ 0 2	[a]
vw	2.030	16	2.025	$\bar{4}$ 0 2	[a]
vw	2.014	17	2.012	$\bar{3}$ 5 1	[a]
vw	1.868	12	1.867	$\bar{1}$ 9 1	[a]
w	1.648	29	1.646	4 6 1	[a]

Notes: The d_{hkl} values were calculated on the basis of the unit cell refined by using single-crystal data. Intensities were calculated on the basis of the structural model using the software Powder Cell (Kraus and Nolze 1996). Observed intensities were visually estimated. s = strong; ms = medium-strong; m = medium; mw = medium-weak; w = weak; vw = very weak. Only reflections with I_{calc} > 5 are listed, if not observed. The five strongest reflections are given in bold. Reflections used for the refinement of the unit-cell parameters are indicated by [a].

CRYSTAL CHEMISTRY OF FERRI-KAERSUTITE

The crystal structure of ferri-kaersutite agrees with the general features of the monoclinic *C*2/*m* amphiboles, which are formed by a double chain of corner-sharing *T*(1) and *T*(2) tetrahedra and a strip of edge-sharing *M*(1), *M*(2), and *M*(3) octahedra, extending in the **c** direction. The *M*(4) site occurs at the junction between the strip of octahedra and the double chain of tetrahedra, whereas the *A* site is located in a large cavity at the center of the hexagonal ring of tetrahedra (Hawthorne and Oberti 2007). The site population of our specimen of ferri-kaersutite was derived by comparing the refined site-scattering values and the unit formula calculated from chemical analyses (Table 7), in agreement with Hawthorne et al. (1995b). Bond-valence balance, calculated following the values given by Brese and O'Keeffe (1991), is reported in Table 8.

The *T* sites

The two independent *T*(1) and *T*(2) sites have average bond distances of 1.672 and 1.638 Å, respectively. The average bond distance for *T*(1) is larger than that for the *T*(2) site, in agreement

[1] Deposit item AM-16-25204, CIF. Deposit items are free to all readers and found on the MSA web site, via the specific issue's Table of Contents (go to http://www.minsocam.org/MSA/AmMin/TOC/).

TABLE 4. Crystal data and summary of parameters describing data collection and refinement for ferri-kaersutite

Crystal data	
Crystal size (mm³)	0.20 × 0.17 × 0.10
Cell setting, space group	Monoclinic, *C*2/*m*
a (Å)	9.8378(8)
b (Å)	18.0562(9)
c (Å)	5.3027(6)
β (°)	105.199(9)
V (Å³)	908.99(13)
Z	2
Data collection and refinement	
Radiation, wavelength (Å)	Mo*K*α, λ = 0.71073
Temperature (K)	293
$2\theta_{max}$ (°)	70.28
Measured reflections	10645
Unique reflections	1924
Data completeness	0.956
Reflections with $F_o > 4\sigma(F_o)$	1783
R_{int}	0.0289
*R*σ	0.0142
Range of indices	$-15 \le h \le 15$, $-29 \le k \le 29$, $-8 \le l \le 8$
R [$F_o > 4\sigma(F_o)$]	0.0385
R (all data)	0.0408
wR (on F_o^2)	0.1125
Goof	1.110
Number of least-squares parameters	111
Maximum peak in the difference-Fourier synthesis (*e* Å⁻³)	0.76 [at 0.67 Å from O(3)]
Maximum hole in the difference-Fourier synthesis (*e* Å⁻³)	−1.13 [at 0.53 Å from *M*(4)]

Notes: The weighting scheme is defined as $w = 1/[\sigma^2(F_o^2) + (aP)^2 + bP]$, with $P = [2F_c^2 + \text{Max}(F_o^2,0)]/3$. *a* and *b* values are 0.0600 and 2.6761.

with the strong tendency of Al to be partitioned at the *T*(1) site in *C*2/*m* amphiboles. Oberti et al. (2007) proposed a linear relation between <*T*(1)–O> and $^{T(1)}$Al, namely $^{T(1)}$Al (apfu) = [<*T*(1)–O> – 1.6193] × 34.2199. By applying this equation, the calculated $^{T(1)}$Al content is 1.803 apfu. Consequently, the proposed site occupancies at the *T*(1) and *T*(2) sites are ($Si_{2.197}Al_{1.803}$) and ($Si_{3.892}Al_{0.108}$), respectively. These site occupancies agree with the bond valence requirements (Table 8). The site-scattering associated with the *T* sites does not indicate any presence of Ti at these sites.

The *M*(1), *M*(2), *M*(3) sites

The total refined site-scattering at the *M*(1), *M*(2), and *M*(3) sites is 75.6 electrons per formula unit (epfu); the total calculated site-scattering of C cations in the formula unit of ferri-kaersutite is 74.6 epfu (Table 7), which is sufficiently close to allow us to derive a site population from the data of Tables 2 and 7.

The average bond distances are 2.067, 2.063, and 2.071 Å for *M*(1), *M*(2), and *M*(3) sites, respectively. Examination of the *M*–*M* distances (Table 6) shows that the *M*(1)–*M*(1) interatomic distance is shorter than the other *M*–*M* distances, indicating that *M*(1) cations are displaced toward the O(3)–O(3) edge, as observed in amphiboles containing significant O^{2-} at the O(3) site and high-charge cations at the *M*(1) site (e.g., mangani-mangano-ungarettiite, Hawthorne et al. 1995a; mangani-obertiite, Hawthorne et al. 2000; mangani-dellaventuraite, Tait et al. 2005; oxo-magnesio-hastingsite, Zaitsev et al. 2013). In addition, following Oberti et al. (2007), the *M*(1)–*M*(2) interatomic distance is sensitive to the presence of an oxo-component at the O(3) site. By using the regression equation derived by Oberti et al. (2007) for pargasite-kaersutite-hastingsite, an $^{O(3)}O^{2-}$ content of 1.26 apfu can be calculated, in good agreement with 1.19 $^{O(3)}O^{2-}$ obtained from chemical analyses. For this reason, all Ti^{4+} was assigned to the *M*(1) site, providing local electroneutrality to the oxo-component at the O(3) site through the substitution $^{M(1)}Ti^{4+} + 2^{O(3)}O^{2-} = {}^{M(1)}(Mg,Fe)^{2+} + 2^{O(3)}OH^-$. The assignment of this element at the *M*(1) site agrees with the relatively larger U_{eq} value compared to those of the other *M* sites (Tiepolo et al. 1999), because Ti does not occupy the same position as Mg, Fe^{2+}, and Fe^{3+}, owing to its typical off-center displacement (e.g., Megaw 1968). The anisotropic displacement ellipsoid of the *M*(1) site is elongated parallel to [010] (see Table 5). In some cases, the splitting of this site has been reported (e.g., Hawthorne et al. 2000). The low value of the octahedral distortion of the *M*(1) site, as defined by Brown and Shannon (1973), suggests a low occupancy by Fe^{3+} at this site, in agreement with Oberti et al. (2007). Consequently, a mixed (Mg,Ti,Fe^{3+}) site occupancy can be proposed at the *M*(1) site. The calculated bond distance is 2.053 Å, compared with the observed value of 2.067 Å.

Hawthorne and Oberti (2007) illustrate the well-developed linear correlation between <*M*(2)–O> and the aggregate size of the constituent cations. By using their relations, an aggregate size of ≈0.69 Å can be obtained, compared with a calculated aggregate size of 0.67 Å resulting from the *M*(2) site population reported in Table 7 and the ionic radii given by Shannon (1976). Consequently, *M*(2) could be a mixed (Mg,Al,Fe^{3+},Cr) site. The calculated bond length, 2.046 Å, is shorter than the observed value, 2.063 Å. It is interesting to note that aluminum is disordered between the *M*(2) and *M*(3) sites, as reported in other mantle amphiboles (e.g., Oberti et al. 1995). Analogously, Cr^{3+} could be disordered over *M*(2) and *M*(3) sites, but its very

TABLE 5. Atomic positions and displacement parameters (in Å²) for ferri-kaersutite

Site	*x*/*a*	*y*/*b*	*z*/*c*	U_{eq}	U_{11}	U_{22}	U_{33}	U_{23}	U_{13}	U_{12}
T(1)	0.28309(5)	0.08524(3)	0.30190(10)	0.0080(1)	0.0077(2)	0.0090(2)	0.0074(2)	−0.0004(1)	0.0024(2)	−0.0009(1)
T(2)	0.29117(5)	0.17265(2)	0.80969(9)	0.0082(1)	0.0077(2)	0.0090(2)	0.0074(2)	0.0004(1)	0.0026(2)	−0.0009(1)
M(1)	0	0.08338(4)	½	0.0131(2)	0.0082(3)	0.0261(4)	0.0062(4)	0	0.0038(2)	0
M(2)	0	0.17695(3)	0	0.0074(2)	0.0074(3)	0.0086(3)	0.0066(4)	0	0.0028(2)	0
M(3)	0	0	0	0.0097(3)	0.0106(4)	0.0099(4)	0.0083(5)	0	0.0021(3)	0
M(4)	0	0.27805(5)	½	0.0145(2)	0.0155(2)	0.0159(4)	0.0148(3)	0	0.0088(2)	0
M(4′)	0	0.2502(12)	½	0.0145(2)	0.0155(2)	0.0159(4)	0.0148(3)	0	0.0088(2)	0
A(*m*)	0.0425(7)	½	0.0838(15)	0.058(2)	0.097(4)	0.022(2)	0.089(4)	0	0.087(3)	0
A(2)	0	0.473(10)	0	0.058(2)	0.097(4)	0.022(2)	0.089(4)	0	0.087(3)	0
O(1)	0.1078(1)	0.08679(7)	0.2192(3)	0.0113(2)	0.0092(5)	0.0140(5)	0.0107(6)	−0.0006(4)	0.0031(4)	−0.0014(4)
O(2)	0.1189(1)	0.17159(7)	0.7278(3)	0.0109(2)	0.0078(4)	0.0142(5)	0.0107(6)	0.0008(4)	0.0025(4)	−0.0003(4)
O(3)	0.1078(2)	0	0.7126(4)	0.0145(3)	0.0117(7)	0.0181(8)	0.0139(9)	0	0.0033(6)	0
O(4)	0.3656(1)	0.25065(7)	0.7878(3)	0.0144(2)	0.0157(5)	0.0127(5)	0.0152(6)	0.0008(4)	0.0047(5)	−0.0039(4)
O(5)	0.3505(1)	0.13952(8)	0.1074(3)	0.0147(3)	0.0113(5)	0.0195(6)	0.0124(6)	0.0061(4)	0.0017(4)	−0.0001(4)
O(6)	0.3469(1)	0.11743(8)	0.6066(3)	0.0153(3)	0.0119(5)	0.0196(6)	0.0147(6)	−0.0058(4)	0.0041(5)	0.0008(4)
O(7)	0.3438(2)	0	0.2802(4)	0.0178(4)	0.0146(8)	0.0154(8)	0.0231(10)	0	0.0044(7)	0

TABLE 6. Selected interatomic distances (in angstroms) and angles (in degrees) for ferri-kaersutite

T(1)	–O(1)	1.665(1)	*T*(2)	–O(4)	1.606(1)	*M*(1)	–O(3)	2.009(1) ×2
	–O(7)	1.666(1)		–O(2)	1.636(1)		–O(1)	2.043(1) ×2
	–O(6)	1.677(1)		–O(5)	1.645(1)		–O(2)	2.150(1) ×2
	–O(5)	1.680(1)		–O(6)	1.662(1)		average	2.067
	average	1.672		average	1.637			
M(2)	–O(4)	1.986(1) ×2	*M*(3)	–O(1)	2.070(1) ×4	*M*(4)	–O(4)	2.325(1) ×2
	–O(2)	2.085(1) ×2		–O(3)	2.072(2) ×2		–O(2)	2.405(2) ×2
	–O(1)	2.116(1) ×2		average	2.071		–O(6)	2.568(2) ×2
	average	2.063					–O(5)	2.666(2) ×2
							average	2.491
M(4′)	–O(2)	2.03(2) ×2	*A*(*m*)	–O(7)	2.444(5)	*A*(2)	–O(7)	2.452(4) ×2
	–O(4)	2.266(1) ×2		–O(7)	2.472(5)		–O(5)	2.652(14) ×2
	average			–O(6)	2.728(6) ×2		–O(6)	2.761(11) ×2
				–O(5)	3.007(3) ×2		average	2.622
				average	2.731			
M(1)–*M*(1)		3.011(2)	*M*(1)–*M*(4′)		3.01(2)	*T*(1)–O(5)–*T*(2)		134.67(9)
M(1)–*M*(2)		3.1439(6)	*M*(2)–*M*(3)		3.1950(6)	*T*(1)–O(6)-*T*(2)		136.78(9)
M(1)–*M*(3)		3.0490(5)	*M*(2)–*M*(4)		3.2190(7)	*T*(1)–O(7)–*T*(1)		135.04(13)

TABLE 7. Refined site scattering values (in electrons per formula unit, epfu) and assigned site populations (in atoms per formula unit, apfu)

Site	Refined site scattering (epfu)	Site population (apfu)	Calculated site scattering (epfu)
M(1)	31.6	$Mg_{1.298}Ti_{0.582}Fe^{3+}_{0.120}$	31.5
M(2)	28.5	$Mg_{1.389}Al_{0.339}Fe^{3+}_{0.261}Cr_{0.011}$	28.1
M(3)	15.5	$Mg_{0.696}Fe^{3+}_{0.116}Al_{0.100}Fe^{2+}_{0.088}$	15.0
M(4) + *M*(4′)	40.4	$Ca_{1.726}Fe^{2+}_{0.258}Mn_{0.014}$	41.6
A(*m*) + *A*(2)	12.5	$Na_{0.816}K_{0.179}$	12.4

TABLE 8. Bond valence sums according to bond-valence parameters taken from Brese and O'Keeffe (1991)

Site	O(1)	O(2)	O(3)	O(4)	O(5)	O(6)	O(7)	Σcations	Theor.
T(1)	0.93				0.89	0.90	$0.92_{\downarrow x2}$	3.64	3.55
T(2)		0.97		1.05	0.95	0.90		3.87	3.97
M(1)	$0.44^{\rightarrow x2}$	$0.33^{\rightarrow x2}$	$0.49^{\rightarrow x2}_{\downarrow x2}$					2.52	2.64
M(2)	$0.32^{\rightarrow x2}$	$0.35^{\rightarrow x2}$		$0.46^{\rightarrow x2}$				2.26	2.31
M(3)	$0.37^{\rightarrow x4}$		$0.37^{\rightarrow x2}$					2.22	2.22
M(4) + *M*(4′)		$0.31^{\rightarrow x2}$		$0.36^{\rightarrow x2}$	$0.14^{\rightarrow x2}$	$0.18^{\rightarrow x2}$		1.98	2.00
A(*m*) + *A*(2)					$0.07^{\rightarrow x2}$	$0.10^{\rightarrow x2}$	$0.17, 0.16, 0.05^{\rightarrow x2}$	0.77	1.00
Σanions	2.06	1.96	1.35	1.87	2.05	2.08	2.22		
Theor.	2.00	2.00	1.60	2.00	2.00	2.00	2.00		

Note: In mixed sites, bond-valence contribution of each cation has been weighted according to its occupancy.

low content does not allow a more accurate determination of the partitioning of this element between the two octahedral sites.

The *M*(3) site hosts Mg, Fe^{3+}, Al, and Fe^{2+}. The latter cation was assigned to this position, owing to its preferential partitioning at the *M*(3) site with respect to *M*(1) and, in particular, to *M*(2) (Oberti et al. 2007). Its calculated average bond distance is 2.050 Å, which is shorter than the observed <*M*(3)–O> value, 2.071 Å.

The *M*(4) site

In ferri-kaersutite, *M*(4) is split into two sub-positions, *M*(4) and *M*(4′); this splitting has been reported by other authors studying amphiboles having a significant amount of ^{B}(Mg, Fe, Mn), e.g., Oberti and Ghose (1993).

M(4) hosts Ca, whereas *M*(4′) is occupied by Fe^{2+} and Mn^{2+}. The coordination of the latter position is characterized by four short distances, ranging from 2.030 to 2.266 Å, and four longer ones (at 2.95 and 2.97 Å). On the contrary, according to Oberti et al. (2007), the coordination of this split sub-positions should be sixfold. In our opinion, this discrepancy may be related to the low accuracy in the determination of the *M*(4′) position, owing to its low site occupancy.

The *A* site

As reported by Hawthorne and Oberti (2007), the A cations do not occupy the central site *A*(2/*m*) but are split into two sub-positions, *A*(*m*) and *A*(2). The former is confined to the mirror plane, whereas the latter is displaced along the [010] direction. The average bond distances of the two sub-positions are 2.731 and 2.622 Å for *A*(*m*) and *A*(2), respectively, suggesting a preferential occupancy of K at the *A*(*m*) site, in agreement with Hawthorne and Oberti (2007). Notwithstanding the difficulty in giving reliable site populations for the split *A* sites, we could hypothesize a mixed (Na,K) site population at the *A*(*m*) position, whereas *A*(2) could be partially occupied by Na only.

GENETIC CONDITIONS OF FERRI-KAERSUTITE

The full characterization of the crystal-chemistry of amphiboles provides an useful tool for unraveling their crystallization conditions. Indeed, the partitioning of Al between *T*(1) and *T*(2) sites as well as the (Mg,Fe) content at the *M*(4′) position are related to the crystallization temperature (Oberti et al. 2007).

The ^{IV}Al partitioning at *T*(2) site, before reaching 2.0 apfu at the *T*(1) site, is a signal of HT conditions of crystallization, while complete Al ordering at *T*(1) suggests temperatures lower than 850 °C (e.g., Perinelli et al. 2012). Ferri-kaersutite agrees with the preferential partitioning of Al at the *T*(1) site; indeed this site has an Al/(Al+Si) atomic ratio close to 0.45, suggesting a crystallization temperature of 850 ± 50 °C. In addition, as stated above, the *M*(4′) site, hosting Mg and Fe^{2+}, is also sensitive to temperature (Oberti et al. 2007). In particular, the ordering of Fe^{2+} at *M*(4′) increases with increasing temperature. This direct correlation, first shown by Oberti et al. (2007), fits well for ferri-kaersutite that contains up to 0.258 apfu of $^{M(4')}Fe^{2+}$, suggesting a relatively high crystallization temperature (~850 °C), consistent with Al partitioning at the tetrahedral sites.

All of these observations are in good agreement with world-wide amphiboles from mantle environments (Oberti et al. 2007), although the chemical composition of ferri-kaersutite indicates uncommonly high oxidizing conditions as well as a low Al content in the bulk system. The temperatures obtained by these unconventional geothermometers based on crystallographic constraints are in agreement with the independent

temperature estimate of 845 ± 30 °C (for n = 8) calculated at a constant pressure of 1.5 GPa using the Opx-Cpx geothermometer proposed by Brey and Kohler (1990) (BKN90). The pressure was chosen taking into account the spinel stability and the mantle silicate parageneses.

Implications

There is a general consensus (e.g., Niu 2008; Pilet et al. 2008) that Ti-rich amphibole (Ti-rich pargasite and kaersutite) plays an important role in the genesis of alkaline magma. In the upper mantle, Ti-rich amphibole commonly occurs as disseminated crystals or veinlets in a peridotite matrix (i.e., Coltorti et al. 2004; Tiepolo et al. 2011) or as large discrete veins structurally isolated by the peridotite matrix (Grégoire et al. 2000). The discovery of a ferric component in the Ti-rich kaersutite group in the upper mantle provides new information about metasomatic redox processes acting in the mantle. The formation of ferri-kaersutite suggests that the Fe^{3+}/Fe_{tot} ratio of the metasomatic silicate melts was high and/or that the volatile-rich melt/fluid percolated through and reacted with the peridotite, concentrating Fe^{3+} and C-O-H volatile species, and increasing Fe^{3+}/Fe_{tot} until the crystallization of ferri-karsutite. The melting of Ti-rich amphibole veins in the lithosphere and subsequent degrees of melt/host peridotite reactions produce melts that can account for the wide compositional spectrum in magmatic products, i.e., from extreme alkaline lavas (i.e., nephelinite, basanite) to the most common alkaline basalts (Fitton and Upton 1987; Pilet et al. 2008). The analyses of volatile contents and the Fe speciation in Ti-rich mantle amphibole is, therefore, crucial to the characterization of the upper mantle redox conditions and volatile circulation, and ultimately sheds light on one of the most intriguing aspects of magma genesis, the volatile contents of the primary magma.

Acknowledgments

The authors thank L. Ottolini (IGG-CNR, Pavia) and R. Carampin (IGG-CNR Padova) for SIMS and EMPA analyses, respectively. M. Coltorti is acknowledged for his fieldwork during PNRA expedition in Northern Victoria Land on 2004. This study was financially supported by the PNRA (Programma Nazionale Ricerche in Antartide) project 2010/A2.08 "Xenoliths and basic lavas in understanding the C-O-H system in the mantle of the polar regions." The paper was handled by the Associate Editor Fernando Colombo and benefited from the careful revisions of Mark Welch and Roberta Oberti.

References cited

Bonadiman, C., Nazzareni, S., Coltorti, M., Comodi, P., Giuli, G., and Faccini, B. (2014) Crystal chemistry of amphiboles: implications for oxygen fugacity and water activity in lithospheric mantle beneath Victoria Land, Antarctica. Contributions to Mineralogy and Petrology, 167, 984–1001.

Brese, N.E., and O'Keeffe, M. (1991) Bond-valence parameters for solids. Acta Crystallographica, B47, 192–197.

Brey, G.P., and Kohler, T.P. (1990) Geothermometry in four-phase lherzolites II: new thermometers and practical assessment of existing thermobarometers. Journal of Petrology, 31, 1353–1378.

Brown, I.D., and Shannon, R.D. (1973) Empirical bond strength-bond length curves for oxides. Acta Crystallographica, A29, 266–282.

Coltorti, M., Beccaluva, L., Bonadiman, C., Faccini, B., Ntaflos, T., and Siena, F. (2004) Amphibole genesis via metasomatic reaction with clinopyroxene in mantle xenoliths from Victoria Land, Antarctica. Lithos, 75, 115–139.

Comodi, P., Boffa Ballaran, T., Zanazzi, P.F., Capalbo, C., Zanetti, A., and Nazzareni, S. (2010) The effect of oxo-component on the high-pressure behavior of amphiboles. American Mineralogist, 95, 1042–1051.

Fitton, J.G., and Upton, B.G.J., Eds. (1987) Alkaline Igneous Rocks. Geological Society Special Publication No 30.

Fitzgerald, P.G., Sandiford, M., Barrett, P.J., and Gleadow, A.J.W. (1987) Asymmetric extention associated with uplift and subsidence in "Transantarctic Mountains and Ross Embayment". Earth and Planetary Science Letters, 81, 67–78.

Gentili, S., Bonadiman, C., Biagioni, C., Comodi, P., Coltorti, M., Zucchini, A., and Ottolini, L. (2015) Oxo-amphiboles in mantle xenoliths: Evidence for H_2O-rich melt interacting with the lithospheric mantle of Harrow Peaks (Northern Victoria Land, Antarctica). Mineralogy and Petrology, 109, 741–759.

Giacomoni, P.P., Coltorti, M., Mukasa, S., Bonadiman, C., Ferlito, C., and Pelorosso, B. (2013) Petrological study of Cenozoic basic lavas and melt inclusions from Northern Victoria Land (Antarctica). Mineralogical Magazine, 77, 1165.

Grégoire, M., Moine, B.N., O'Reilly, S.Y., Cottin, J.Y., and Giret, A. (2000) Trace element residence and partitioning in mantle xenoliths metasomatized by high alkaline silicate and carbonate-rich melts (Kerguelen Islands, Indian Ocean). Journal of Petrology, 41, 477–509.

Hawthorne, F.C., and Oberti, R. (2007) Amphiboles: Crystal chemistry. Reviews in Mineralogy and Geochemistry, 67, 1–51.

Hawthorne, F.C., Oberti, R., Cannillo, E., Sardone, N., Zanetti, A., Grice, J.D., and Ashley, P.M. (1995a) A new anhydrous amphibole from the Hoskins mine, Grenfell, New South Wales, Australia: Description and crystal structure of ungarettiite, $NaNa_2(Mn^{2+}_2Mn^{3+}_3)Si_8O_{22}O_2$. American Mineralogist, 80, 165–172.

Hawthorne, F.C., Ungaretti, L., and Oberti, R. (1995b) Site populations in minerals: terminology and presentation of results of crystal-structure refinement. Canadian Mineralogist, 33, 907–911.

Hawthorne, F.C., Cooper, M.A., Grice, J.D., and Ottolini, L. (2000) A new anhydrous amphibole from the Eifel region, Germany: Description and crystal structure of obertiite, $NaNa_2(Mg_3FeTi)Si_8O_{22}O_2$. American Mineralogist, 85, 236–241.

Hawthorne, F.C., Ball, N.A., and Czamanske. G.K. (2010) Ferro-obertiite $NaNa_2(Fe^{2+}_3Fe^{3+}Ti)Si_8O_{22}O_2$, a new mineral species of the amphibole group from Coyote Peak, Humboldt Country, California. Canadian Mineralogist, 401, 301–306.

Hawthorne, F.C., Oberti, R., Harlow, G.F., Maresch, W.V., Martin, R.F., Schumacher, J.C., and Welch, M.D. (2012) Nomenclature of the amphibole supergroup. American Mineralogist, 97, 2031–2048.

Holland, T.J.B., and Redfern, S.A.T. (1997) Unit cell refinement from powder diffraction data: The use of regression diagnostics. Mineralogical Magazine, 61, 65–77.

Kraus, W., and Nolze, G. (1996) POWDER CELL—a program for the representation and manipulation of crystal structures and calculation of the resulting X-ray powder patterns. Journal of Applied Crystallography, 29, 301–303.

Megaw, H.D. (1968) A simple theory of the off centre displacement of cations in octahedral environments. Acta Crystallographica, B24, 149–153.

Melchiorre, M., Coltorti, M., Bonadiman, C., Faccini, B., O'Reilly, S.Y., and Pearson, N.J. (2011) The role of eclogite in the rift-related metasomatism and Cenozoic magmatism of Northern Victoria Land, Antarctica. Lithos, 124, 319–330.

Mercier, J.C., and Nicolas, A. (1975) Textures and fabrics of upper mantle peridotites as illustrated by xenoliths from basalts. Journal of Petrology, 16, 454–487.

Niu, Y. (2008) The Origin of Alkaline Lavas. Science, 320, 883–884.

Oberti, R., and Ghose, S. (1993) Crystal-chemistry of a complex Mn-bearing alkali amphibole ("tirodite") on the verge of exsolution. European Journal of Mineralogy, 5, 1153–1160.

Oberti, R., Hawthorne, F.C., Ungaretti, L., and Cannillo, E. (1995) $^{[6]}$Al disorder in amphiboles from mantle peridotites. Canadian Mineralogist, 33, 867–878.

Oberti, R, Hawthorne, F.C., Cannillo, E., and Càmara, F. (2007) Long-range order in amphiboles. Reviews in Mineralogy and Geochemistry, 67, 125–171.

Oberti, R., Zanetti, A., Boiocchi, M., Hawthorne, F.C., and Ball, N.A. (2015) Oxo-manganileakeite, IMA 2015-035. CNMNC Newsletter No. 26, August 2015, p. 945. Mineralogical Magazine, 79, 941–947.

Ottolini, L., Bottazzi, P., and Vannucci, R. (1993) Quantification of lithium, beryllium and boron in silicates by secondary ion mass spectrometry using conventional energy filtering. Analytical Chemistry, 65, 1960–1968.

Ottolini, L., Bottazzi, P., Zanetti, A., and Vannucci, R. (1995) Determination of hydrogen in silicates by secondary ion mass spectrometry. The Analyst, 120, 1309–1314.

Ottolini, L., Cámara, F., and Hawthorne, F.C. (2001) Quantification of H, B, F in kornerupine: Accuracy of SIMS and SREF (X-ray single-crystal structure refinement) data. Microchimica Acta, 20, 1–5.

Ottolini, L., Cámara, F., Hawthorne, F.C., and Stirling, J. (2002) SIMS matrix effects in the analysis of light elements in silicate minerals: Comparison with SREF and EMPA data. American Mineralogist, 87, 1477–1485.

Perinelli, C., Armienti, P., and Dallai, L. (2006) Geochemical and O-isotope constraints on the evolution of lithospheric mantle in the Ross Sea rift area (Antarctica). Contributions to Mineralogy and Petrology, 151, 245–266.

Perinelli, C., Andreozzi, G.B., Conte, A.M., Oberti, R., and Armienti, P. (2012) Redox state of subcontinental lithospheric mantle and relationships with metasomatism: insights from spinel peridotites from northern Victoria Land (Antarctica). Contributions to Mineralogy and Petrology, 164, 1053–1067.

Pilet, S., Baker, M.B., and Stolper, E.M. (2008) Metasomatized lithosphere and the origin of alkaline lavas. Science, 320, 916–919.

Pouchou, J.L., and Pichoir, F. (1985) "PAP" (φ-ρ-Z) procedure for improved quantitative microanalysis. In J.T. Armstrong, Ed., Microbeam Analysis, p.

104–106. San Francisco Press, California.
Prescher, C., McCammon, C., and Dubrovinsky, L. (2012) MossA—a program for analyzing energy-domain Mössbauer spectra from conventional and synchrotron source. Journal of Applied Crystallography, 45, 329–331.
Rocchi, S., Armienti, P., D'Orazio, M., Tonarini, S., Wijbrans, J., and Di Vincenzo, G. (2002) Cenozoic magmatism in the western Ross Embayment: role of mantle plume vs. plate dynamics in the development of the West Antarctic rift system. Journal of Geophysical Research, 107, DOI: 10.1029/2001JB000515.
Shannon, R.D. (1976) Revised effective ionic radii and systematic studies of interatomic distances in halides and chalcogenides. Acta Crystallographica, A32, 751–767.
Sheldrick, G.M. (2008) A short history of SHELX. Acta Crystallographica, A64, 112–122.
Tait, K.T., Hawthorne, F.C., Grice, J.D., Ottolini, L., and Nayak, V.K. (2005) Dellaventuraite, $NaNa_2(MgMn_2^{3+}Ti^{4+}Li)Si_8O_{22}O_2$, a new anhydrous amphibole from the Kajlidongri Manganese Mine, Jhabua District, Madhya Pradesh, India. American Mineralogist, 90, 304–309.
Tiepolo, M., Zanetti, A., and Oberti, R. (1999) Detection, crystal-chemical mechanism and petrological implications of $^{[6]}Ti^{4+}$ partitioning in pargasite and kaersutite. European Journal of Mineralogy, 11, 345–354.
Tiepolo, M., Tribuzio, R., and Langone, A. (2011) High-Mg andesite petrogenesis by amphibole crystallization and ultramafic crust assimilation: Evidence from Adamello Hornblendites (Central Alps, Italy). Journal of Petrology, 52, 1011–1045.
Wilson, A.J.C. (1992) International Tables for Crystallography Volume C. Kluwer, Dordrecht.
Wörner, G. (1999) Lithospheric dynamics and mantle sources of alkaline magmatism of the Cenozoic West Antarctic Rift System. Global and Planetary Change, 23, 61–77.
Zaitsev, A.N., Avdontseva, E.Y., Britvin, S.N., Demény, A., Homonnay, Z., Jeffries, T., Keller, J., Krivovichev, V.G., Markl, G., Platonova, N.V., Siidra, O.I., and Spratt, J. (2011) Ferrikaersutite, IMA 2011-035. CNMNC Newsletter No. 10, October 2011, p. 2556. Mineralogical Magazine, 75, 2549–2561.
Zaitsev, A.N., Avdontseva, E.Y., Britvin, S.N., Demény, A., Homonnay, Z., Jeffries, T., Keller, J., Krivovichev, V.G., Markl, G., Platonova, N.V., and others. (2013) Oxo-magnesio-hastingsite, $NaCa_2(Mg_2Fe_3^{3+})(Si_6Al_2)O_{22}O_2$, a new anhydrous amphibole from the Deeti volcanic cone, Gregory rift, northern Tanzania. Mineralogical Magazine, 77, 2773–2792.
Zipfel, J., and Wörner, G. (1992) Four- and five-phase peridotites from a continental rift system: evidence for upper mantle uplift and cooling at the Ross Sea margin (Antarctica). Contributions to Mineralogy and Petrology, 111, 24–36.

Manuscript received September 29, 2014
Manuscript accepted September 1, 2015
Manuscript handled by Fernando Colombo